25th ABCM International Congress of Mechanical Engineering
October 20-25, 2019, Uberlândia, MG, Brazil

COB-2019-1168
NUMERICAL ANALYSIS OF DEFORMATION AND BREAKUP OF A THREE-DIMENSIONAL DROPLET

Victor Guinancio e Abicalil
Taygoara Felamingo de Oliveira
Laboratório de Energia e Ambiente, Universidade de Brasília
victorabicalil@gmail.com
taygoara@unb.br

Abstract. *This work presents numerical simulations of incompressible multiphase flows, with an emphasis on droplet deformation and breakup in simple shear flows. This is achieved through use of the Level Set method to capture the interface between the two phases, alongside a projection method to simulate the fluid flow, with time steps performed with the Crank-Nicolson method and a finite difference scheme for spacial discretization. The method is validated by comparing droplet deformation and inclination angle for varying Capillary number and viscosity ratios with theoretical, numerical and experimental results available in the literature, with good agreement. Simulations were performed with viscosity ratios ranging between* 0.3 *and* 35*. Some droplet breakup simulations are also presented.*

Keywords: *multiphase flow, Level Set method, droplet deformation, droplet breakup.*

1. INTRODUCTION

Multiphase flows are an integral part in a wide variety of engineering applications, such as some types of turbines, fuel injection systems, inkjet printers, evaporators and condensers, among others, and also happens in a wide variety of scales. In this work, however, our focus is on the study of emulsions, from a microscopic point of view. As such, we will focus on studying the flows developed around droplets of one fluid immersed in another fluid, in the case of immiscible fluids, instead of analyzing emulsions as a single fluid in a macroscopic scale. The study of these flows is paramount for understanding the process of formation of emulsions, and to characterize the behaviour of such emulsions.

The subject of droplet deformation and breakup has been the subject of many previous works, utilizing theoretical, experimental and numerical methods, dating back to the classical work of Taylor (1932). Current works focus on more complex systems, such as the compound droplets analyzed by Vu *et al.* (2019), magneto-rheological droplets under magnetic fields studied by Hassan *et al.* (2018) and Cunha *et al.* (2018), and the multiple droplet systems studied by Barai and Mandal (2019).

In the present work, simulations are performed with the Level Set method, initially proposed by Osher and Sethian (1988), which is capable of dealing with drastic geometry changes, such as the breakup of droplets, in an automatic fashion, and also allows for a straightforward calculation of the curvature of the droplet surface. A good review on the Level Set method and its main applications is presented by Gibou *et al.* (2018).

2. METHODOLOGY

In this work, simulations were conducted for simple shear flows, with one single droplet of one fluid (dispersed phase) immersed in another fluid (matrix phase). This is achieved by performing simulations in the computational domain represented in Fig. 1, of dimensions $L_X \times L_Y \times L_Z$, with one initially spherical droplet of radius r_d placed in its center. A droplet deformed by the flow will no longer be spherical, and will have a length L, a breadth B, and an inclination angle θ. L, B and θ are all measured in the plane normal to Z that passes through the droplet center.

The walls normal to the Y axis move in the X direction, with velocities of $U/2$ and $-U/2$ for the upper and lower walls, respectively, resulting in an average shear rate of $\dot{\gamma}_c = U/H$. Velocity boundary conditions on these walls are all Dirichlet, corresponding to the no-slip condition, while pressure boundary conditions are homogeneous Neumann. All other boundary conditions are periodic.

For fluids with density ρ, viscosity μ_d for the dispersed phase, viscosity μ_m for the matrix phase, and a surface tension coefficient of γ between them, one can define the Reynolds number as $Re = \rho\dot{\gamma}_c r_d^2/\mu_m$, the Capillary number as $Ca = r_d\dot{\gamma}_c\mu_m/\gamma$, and the viscosity ratio as $\lambda = \mu_d/\mu_m$. In the case of high viscosity ratios, it is useful to use auxiliary nondimensional parameters, in order to improve numerical stability. For viscosity ratios less than or equal to 1, the

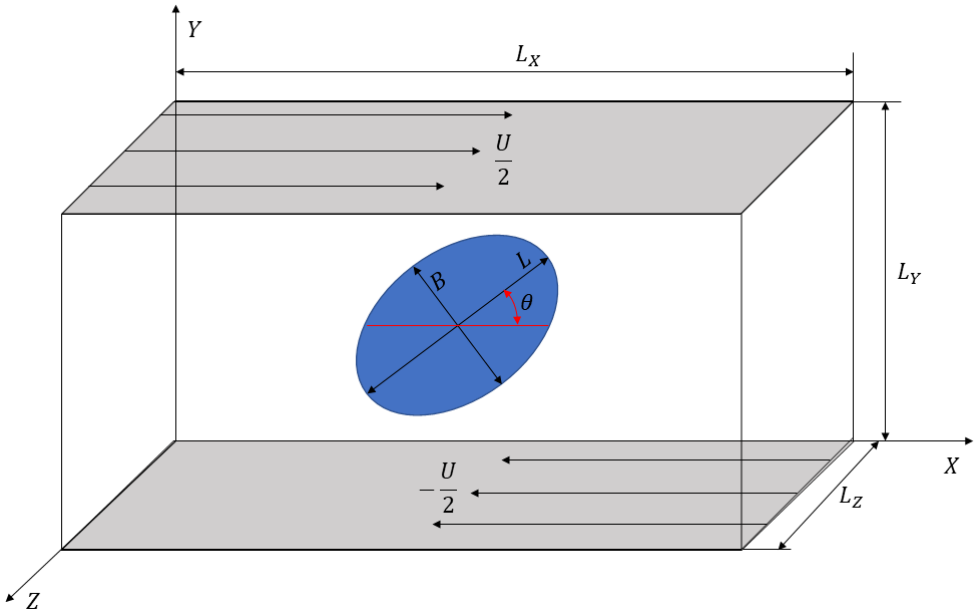

Figure 1: Schematic of a droplet immersed in a simple shear flow.

nondimensional parameters remain the same: $Re_{aux} = Re$, $Ca_{aux} = Ca$ and $\lambda_{aux} = \lambda$. For the case of viscosity ratios greater than 1, however, the reference viscosity is taken as the droplet viscosity, so that $Re_{aux} = Re/\lambda$, $Ca_{aux} = \lambda Ca$, and $\lambda_{aux} = 1/\lambda$. The reasoning behind this choice will be discussed in further detail later in this section.

The flow is governed by the incompressible Navier-Stokes equations, with the addition of a body force term accounting for the surface tension at the droplet surface. (Sussman *et al.*, 1994):

$$\frac{\partial \mathbf{u}}{\partial t} + \mathbf{u} \cdot \nabla \mathbf{u} = -\nabla P + \frac{1}{Re} \nabla \cdot (\mu(\nabla \mathbf{u} + \nabla \mathbf{u}^T)) - \frac{1}{ReCa} \kappa \delta(d) \hat{\mathbf{n}} \,, \tag{1}$$

$$\nabla \cdot \mathbf{u} = 0 \,, \tag{2}$$

where $\mathbf{u}$ is the velocity field, P is the pressure, μ the nondimensional viscosity, κ is the local mean curvature of the droplet surface, δ is the Dirac Delta function, d is the normal distance to the droplet surface, and $\hat{\mathbf{n}}$ is a unit vector normal to the droplet surface. It is clear that in this formulation, the surface tension is zero everywhere except on the interface between the two fluids.

In order to solve the Navier-Stokes equations, the projection method proposed by Kim and Moin (1985) is used with some modifications. This method consists in computing a tentative velocity field, $\mathbf{u}^*$, without the influence of pressure, based on Eq. 1, and then correcting this field to find the true, incompressible, velocity field. As such, this method imposes the incompressibility constraint on every single time step, and the pressure field can be understood as a Lagrange multiplier to force the incompressible flow constraint.. The equation for the tentative velocity field, based on the Crank-Nicolson method, is

$$\frac{\mathbf{u}^* - \mathbf{u}^n}{\Delta t} = \mathbf{A}^{n+\frac{1}{2}} + \frac{1}{2Re} \nabla^2 \mathbf{u}^* - \frac{1}{2Re} \nabla^2 \tilde{\mathbf{u}}^{n+1} \,, \tag{3}$$

where

$$\mathbf{A} = -\mathbf{u} \cdot \nabla \mathbf{u} + \frac{1}{Re} \nabla \cdot (\mu(\nabla \mathbf{u} + \nabla \mathbf{u}^T)) - \frac{1}{ReCa} [\kappa \delta(d) \hat{n}] \,. \tag{4}$$

In Eq. 3, $\tilde{\mathbf{u}}^{n+1}$ is an extrapolation of $\mathbf{u}$ at the $n+1$ instant, calculated as $\tilde{\mathbf{u}}^{n+1} = 2\mathbf{u}^n - \mathbf{u}^{n-1}$, and the term $\mathbf{A}^{n+\frac{1}{2}}$ is extrapolated as $\mathbf{A}^{n+\frac{1}{2}} = \frac{3}{2}\mathbf{A}^n - \frac{1}{2}\mathbf{A}^{n-1}$. Since Eq. 3 is based on a Crank-Nicolson scheme, the present method is of second order in time and possesses good stability characteristics. The true velocity field, $\mathbf{u}^{n+1}$, is then calculated as

$$\mathbf{u}^{n+1} = \mathbf{u}^* - \Delta t \nabla \chi^{n+1} \,, \tag{5}$$

where χ is an auxiliary variable closely related to pressure. By taking the divergence of Eq. 5 and applying the incompressibility constraint, we find that

$$\nabla^2 \chi^{n+1} = \frac{1}{\Delta t} \nabla \cdot \mathbf{u}^* \,. \tag{6}$$

Finally, by combining Eqs. 3 and 5, taking the limit of $\Delta t \to 0$ and comparing the resulting equation with Eq. 1, we find that the true pressure, P, is defined as

$$P^{n+\frac{1}{2}} = \chi^{n+1} + \frac{\Delta t}{2Re}\nabla^2\chi^{n+1}\,. \tag{7}$$

In order to track the interface between the two fluids, the Level Set method is used, as proposed by Sussman *et al.* (1994) for the case of incompressible, two-phase flow. This method consists in creating a scalar field ϕ, called the Level Set function, initially set as a signed distance function from the interface. In this way, the Level Set function has positive values outside of the droplet, negative values inside the droplet, and the interface can be defined as the region where the Level Set function is equal to zero. The terms relative to the surface tension component of Eq. 1 can be rewritten in function of ϕ: the unit vector normal to the droplet surface can be defined as $\hat{n} = \frac{\nabla\phi}{|\nabla\phi|}$, the curvature can be defined as $\kappa = \nabla\cdot\hat{n}$, and $\delta(d) = \delta_\epsilon(\phi)|\nabla\phi|$ (Osher and Fedkiw, 2006), with the smoothed Dirac Delta function defined as

$$\delta_\epsilon(\phi) = \begin{cases} 0, & \text{if } \phi < -\epsilon \\ \frac{1}{2\epsilon}[1+\cos(\frac{\pi\phi}{\epsilon})], & \text{if } |\phi| \le \epsilon \\ 0, & \text{if } \phi > \epsilon\,, \end{cases} \tag{8}$$

$$\epsilon = \frac{3}{2}\max(\Delta x, \Delta y, \Delta z)\,. \tag{9}$$

It can be seen from Eq. 8 that the thickness of the interface between the fluids is equal to $2\epsilon/|\nabla\phi|$. Since a uniform interface thickness is essential for the numerical stability of the method, it is desirable that ϕ remains close to a signed distance function, that is, $|\nabla\phi| \approx 1$. The nondimensional viscosity μ in Eqs. 1 and 4 can be defined as

$$\mu = \begin{cases} \lambda_{aux} + (1-\lambda_{aux})H_\epsilon(\phi), & \text{if } \lambda \le 1 \\ \lambda_{aux} + (1-\lambda_{aux})H_\epsilon(-\phi), & \text{if } \lambda > 1\,, \end{cases} \tag{10}$$

with the smoothed Heaviside function H_ϵ defined as

$$H_\epsilon(\phi) = \begin{cases} 0, & \text{if } \phi < -\epsilon \\ \frac{1}{2}[1+\frac{\phi}{\epsilon}+\frac{1}{\pi}\sin(\frac{\pi\phi}{\epsilon})], & \text{if } |\phi| \le \epsilon \\ 1, & \text{if } \phi > \epsilon\,. \end{cases} \tag{11}$$

As evidenced by Eq. 10, large values of λ_{aux} would result in very large viscosity gradients across the droplet interface, which would be a cause of severe numerical instability. As such, the use of the auxiliary nondimensional parameters previously discussed is essential in the case of large λ, as it ensures that $\lambda_{aux} \le 1$, and thus limits the viscosity gradients to manageable values.

In order to accurately capture the interface as the flow develops, the Level Set function needs to be transported by the flow. This is achieved with an advection equation (Sussman *et al.*, 1994):

$$\frac{\partial\phi}{\partial t} = -\mathbf{u}\cdot\nabla\phi\,. \tag{12}$$

Equation 12 ensures that the value of the Level Set function is conserved on material particles, that is, a given material particle will have a fixed value of ϕ as it is transported by the flow. As such, the interface, defined as the points where the Level Set function has a fixed value ($\phi(\mathbf{x}) = 0$), is accurately transported by the flow. Since the velocity fields are not uniform, however, the material particles in which $\phi \neq 0$ will not remain at a fixed distance to the interface. This means that, over time, the Level Set function diverges substantially from a signed distance function, leading to miscalculations of the interface shape functions, such as its curvature and normal vector. Therefore, it is necessary to periodically modify the Level Set function so that it becomes a closer approximation to a signed distance function, without moving the interface. This process is called re-initialization, and in the present work is performed by solving the so called reinitialization equation, first proposed by Sussman *et al.* (1994). A collateral effect of this reinitialization process is that numerical errors can cause significant fluctuations in the dispersed phase volume over time. These volume fluctuations can be mitigated with modifications to the reinitialization equation, as proposed by Sussman *et al.* (1998), by locally imposing a conservation of volume. This modified reinitialization equation is defined as

$$\frac{\partial\phi}{\partial\tau} = S_\epsilon(\phi)(1-|\nabla\phi|) + \lambda_{ijk}f(\phi)\,, \tag{13}$$

$$\lambda_{ijk} = -\frac{\int_{\Omega_{ijk}}\delta_\epsilon(\phi)S_\epsilon(\phi)(1-|\nabla\phi|)dV}{\int_{\Omega_{ijk}}\delta_\epsilon(\phi)f(\phi)dV}\,, \tag{14}$$

$$f(\phi) = \delta_\epsilon(\phi)|\nabla\phi|\,, \tag{15}$$

where Ω_{ijk} is an individual grid cell, and S_ϵ is a smoothed signum function. In the present work, we use the smoothed signum function proposed by Peng *et al.* (1999),

$$S_\epsilon = \frac{\phi}{\sqrt{\phi^2 + |\nabla\phi|^2 \max(\Delta x, \Delta y, \Delta z)^2}}\,, \tag{16}$$

which changes the convergence speed of Eq. 13 depending on the values of $|\nabla\phi|$. This speeds up the convergence when the Level Set function is flat, and improves stability when the Level Set function is steep.

The volume of the computational domain is discretized with the Finite Difference method. Spacial derivatives for the Navier-Stokes equations are all centered with a two-point stencil, and thus second order, with the exception of the derivatives associated with the advection term, which are calculated with a second-order ENO (Essentially Non-Oscillatory) scheme, as described by Osher and Fedkiw (2006), and upwinding. Time steps for the Level Set advection and re-initialization equations are performed with a third-order TVD (Total Variation Diminishing) Runge-Kutta scheme, proposed by Shu and Osher (1988), and the spacial derivatives are calculated with a fifth-order WENO (Weighted Essentially Non-Oscillatory) scheme, proposed by Jiang and Shu (1996), and upwinding. This high level of accuracy is necessary because the Level Set method is very sensitive to numerical errors.

3. RESULTS

3.1 Code Validation

Before any further investigations with the computational code written based on the numerical methodology presented, it is first necessary to validate it. This was performed both for the case of single-phase flow on a lid driven cavity, and the two-phase, simple shear flow described before.

For the case of single-phase flow, order analyses were performed to ensure that the results correctly matched the second-order of both the time and spacial discretization of the numerical methodology utilized. Then, to make sure that our code is accurate, simulations of a lid-driven cavity were performed for varying cavity geometry and Reynolds numbers, with our results compared against the benchmark data of Albensoeder and Kuhlmann (2005) and displaying excellent agreement.

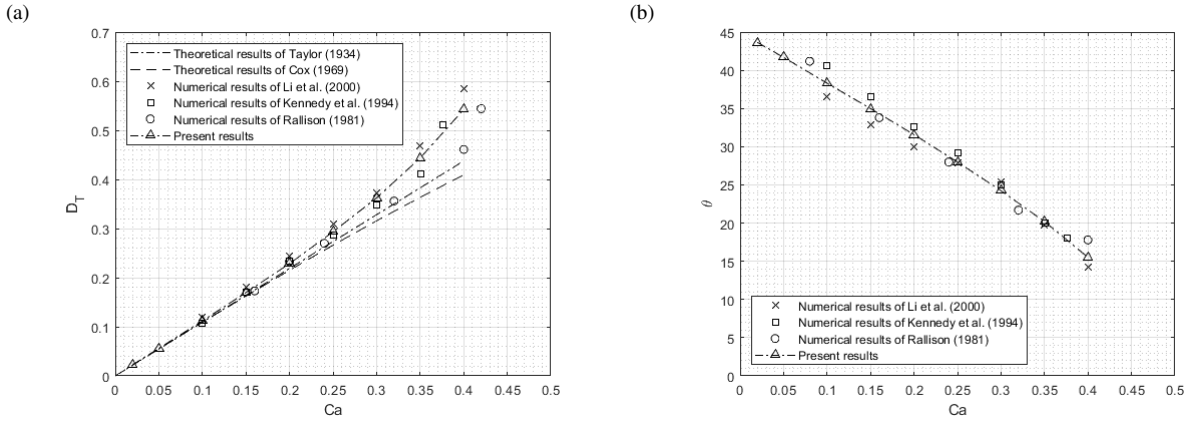

Figure 2: Analysis of droplet deformation and inclination for varying Capillary number. Stokes flow, $\lambda = 1$. (a) Taylor deformation parameter; (b) Droplet inclination.

For the case of the two-phase simple-shear flow, the accuracy of our code was measured by comparing the Taylor deformation parameter and droplet inclination of our results with data available in the literature, for varying Capillary number and viscosity ratios. First, we compare our results for $\lambda = 1$ with the theoretical models presented by Taylor (1934) and Cox (1969), as well as the Boundary Integral method results of Rallison (1981) and Kennedy *et al.* (1994), and the Volume of Fluid method results of Li *et al.* (2000). The results are presented for varying Capillary numbers and Stokes flow ($Re = 0$). The Taylor deformation parameter is defined as

$$D_T = \frac{L - B}{L + B}\,, \tag{17}$$

where L is the droplet length, and B is its breadth. A spherical undeformed droplet will have equal length and breadth, resulting in $D_T = 0$, while the limit case of an infinitely stretched droplet ($B = 0$) results in $D_T = 1$. Inclination angle is defined as the angle between the longest axis of the droplet and the principal direction of the flow.

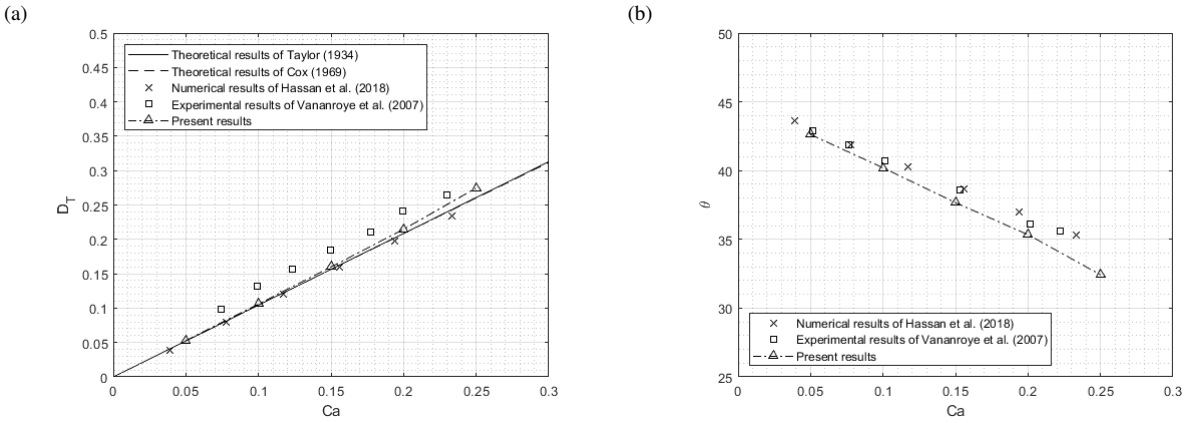

Figure 3: Analysis of droplet deformation and inclination for varying Capillary number. Stokes flow, $\lambda = 0.3$. (a) Taylor deformation parameter; (b) Droplet inclination.

In Fig. 2, it can be seen that there is a good agreement between our results and data available in the literature. Our simulations for $\lambda = 1$ were performed with a mesh of $86 \times 86 \times 43$ for a $8 \times 8 \times 4$ domain. In the case of $\lambda = 0.3$, Fig. 3 shows a comparison between our results and data available in the literature, for varying Capillary numbers and Stokes flow ($Re = 0$). Our results are for a $6 \times 6 \times 6$ domain with a $48 \times 48 \times 48$ mesh, and are presented alongside the theoretical results of Taylor (1934) and Cox (1969), as well as the numerical results of Hassan *et al.* (2018) and the experimental results of Vananroye *et al.* (2007). Again, we find good agreement between our results and data available in the literature.

For the case of high viscosity ratios, the droplet dynamics become considerably different, with the droplet taking a very long time to reach a steady-state shape, due to the occurrence of a tumbling phenomenon. In this tumbling motion, the droplet rotates, with significant oscillations in both its deformation and inclination angle, reminiscent to those of an underdamped dynamic system (Fig. 4). It can also be seen that very viscous droplets tend to align to the flow direction, that is, $\theta \approx 0$.

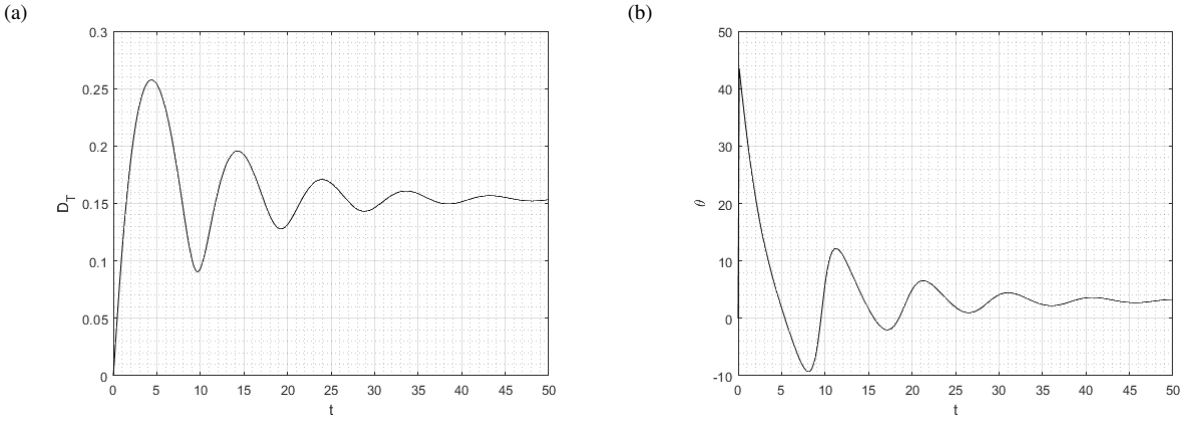

Figure 4: Analysis of droplet deformation and inclination over time, Stokes flow, $Ca = 1$, $\lambda = 10$. (a) Taylor deformation parameter; (b) Droplet inclination.

Figure 5 shows a comparison between our results, for a $6 \times 6 \times 6$ domain with a $48 \times 48 \times 48$ mesh, and some theoretical models available in the literature, namely the very high viscosity ratio models of Taylor (1934) and Oliveira and Cunha (2015), and the very comprehensive model of Cox (1969). It can be seen that, in the case of $Ca = 1$, there is overall a good agreement between all three theoretical models and our results. In the case of $Ca = 0.1$, however, there is some disagreement between the theoretical models for $\lambda < 20$. This is to be expected, given that both the models of Taylor and Oliveira and Cunha were developed solely for the case of very viscous droplets ($\lambda \to \infty$), and as such were extrapolated beyond their intended scope of use, at such a low Capillary number. The model of Cox is the most comprehensive one, and the only of the three actually suitable for these circumstances. It is also the one with which our results have the best agreement. For $\lambda > 20$ there is a good agreement between all three models and our numerical results.

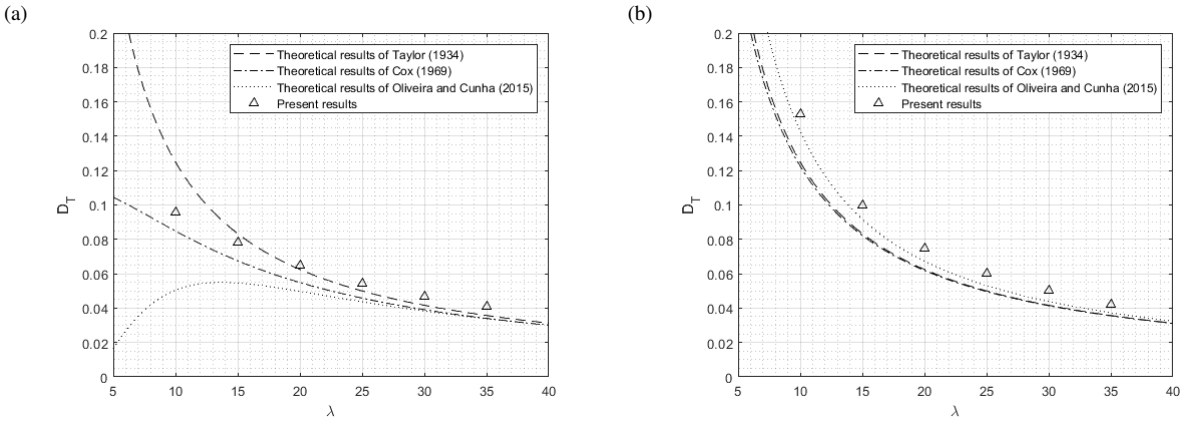

Figure 5: Analysis of droplet deformation for varying viscosity ratios, Stokes flow. (a) $Ca = 0.1$; (b) $Ca = 1$.

3.2 Droplet Breakup

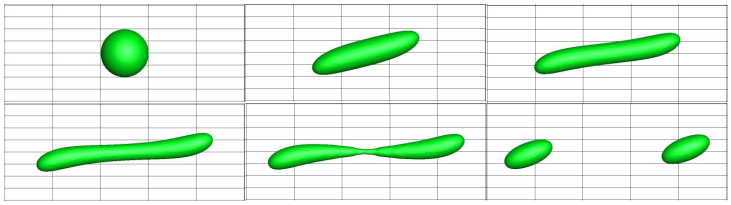

Figure 6: Droplet breakup under simple shear flow. $Re = 0.1$, $Ca = 0.45$, $\lambda = 1$. Without volume conservation constraint, 40% volume loss of the dispersed phase. From upper left to lower right: $t = 0$, $t = 5$, $t = 10$, $t = 15$, $t = 20$ and $t = 25$.

Figure 6 shows a process of droplet breakup under shear flow, with $Re = 0.1$, $Ca = 0.45$ and $\lambda = 1$. This simulation was performed on a somewhat coarse mesh ($120 \times 48 \times 48$ grid for a $10 \times 4 \times 4$ domain), and without imposing the volume conservation constraint in the reinitialization equation. The use of such a mesh without imposing the volume conservation constraint resulted in a loss of dispersed phase volume of nearly 40%. As such, the results of this simulation are presented solely as a demonstration of the importance of using the volume conservation constraint.

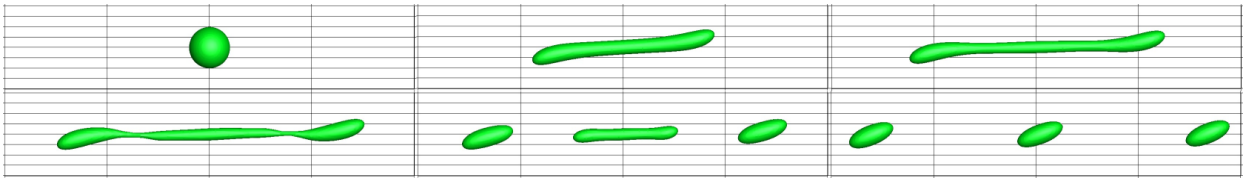

Figure 7: Droplet breakup under simple shear flow. $Re = 0.1$, $Ca = 0.45$, $\lambda = 1$. With volume conservation constraint, volume fluctuations of the dispersed phase were kept to within 1%. From upper left to lower right: $t = 0$, $t = 15$, $t = 25$, $t = 35$, $t = 40$ and $t = 55$.

As a comparison, Fig. 7 shows a simulation with the same parameters on a mesh of equivalent refinement ($240 \times 48 \times 48$ for a $20 \times 4 \times 4$ domain), but with volume fluctuations of the dispersed phase of only 1%, thanks to the use of the volume conservation constraint in the reinitialization equation. The use of a longer domain was necessary to accommodate the larger droplet deformation. It can be seen that the volume loss drastically changes the results. In Fig. 6, there is a large volume loss in the neck formed in the center of the droplet, which causes the breakup to occur prematurely and prevents the formation of a third, center droplet. In Fig. 7, in comparison, the droplet takes significantly longer to breakup, and is stretched much farther. This results in the formation of three droplets, as opposed to just two in Fig. 6.

Figure 8 shows the breakup of a droplet with $Re = 15$, $Ca = 0.15$ and $\lambda = 1$, with a mesh of $144 \times 96 \times 48$ for a $12 \times 8 \times 4$ domain. With the use of the volume conservation constraint in the reinitialization equation, the dispersed phase volume had a 4% increase. Comparing our results to the numerical results of Croce *et al.* (2010), it can be seen that both are very similar up until the point of breakup. After the droplet breakup, however, our results show the formation of a small satellite droplet in the center, while in the results of Croce *et al.* (2010) there is no satellite droplet. As evidenced

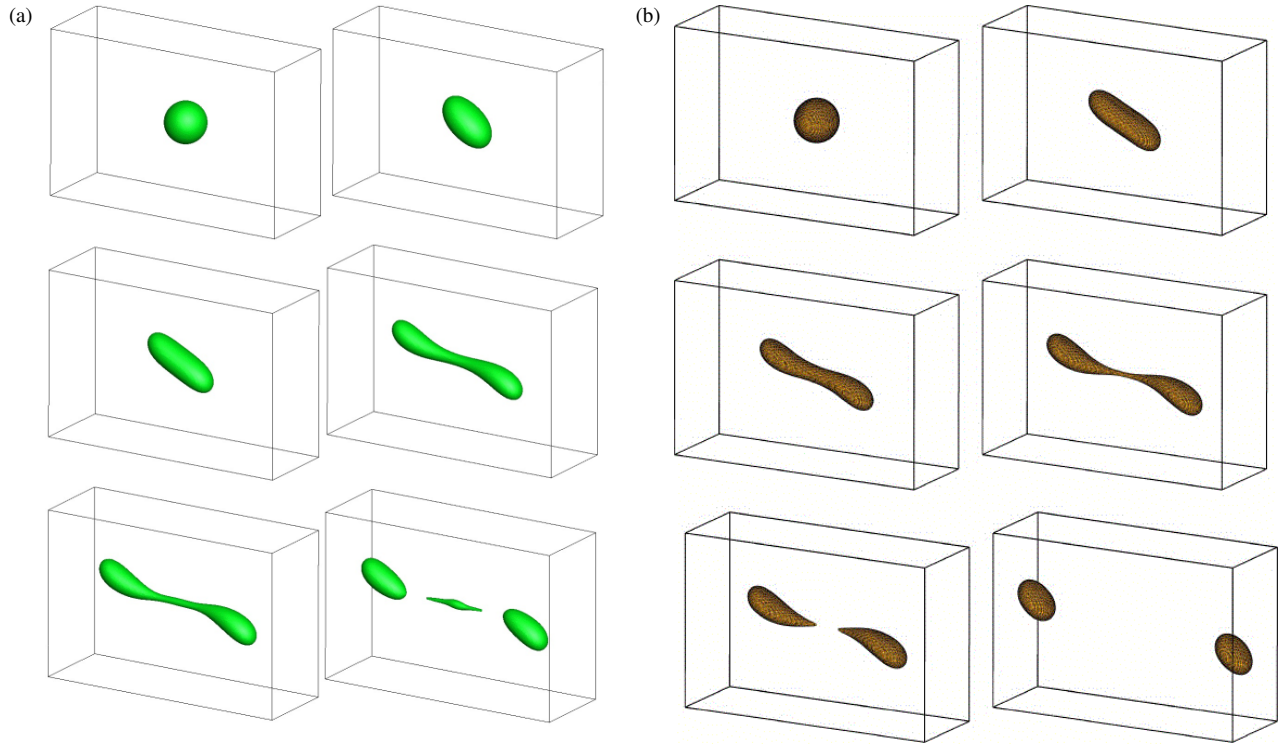

Figure 8: Droplet breakup under simple shear flow. $Re = 15$, $Ca = 0.15$, $\lambda = 1$. (a) Present results (from upper left to lower right: $t = 0$, $t = 50$, $t = 75$, $t = 90$, $t = 92.5$ and $t = 95$); (b) Numerical results of Croce *et al.* (2010).

by the timestamps, the droplet deformation has a very long transient phase, but the breakup itself is quite abrupt.

Finally, Fig. 9 shows a droplet in a confined simple shear with $Re = 0.01$, $Ca = 0.6$, $\lambda = 11.7$ and $2r_d/L_Y = 0.75$. In this figure, the upper wall moves from right to left, and the lower wall moves from left to right. In the absence of wall effects, this droplet would not break up, as indicated by Fig. 5, in which droplets reach a steady state at lower viscosity ratio and higher Capillary number. In fact, in the absence of wall effects, droplets with a viscosity ratio greater than 3.5 do not breakup, regardless of Capillary number (Grace, 1982). However, under significant confinement, breakup of very viscous droplets is possible, as demonstrated by the experimental results of Vananroye *et al.* (2006), against which our results are compared in Fig. 9. It can be seen that our results are qualitatively very similar, including the formation of a single satellite droplet in the center.

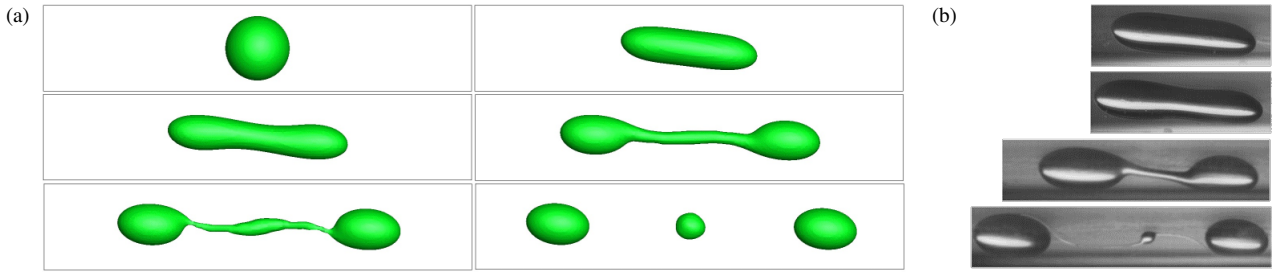

Figure 9: Droplet breakup under confined simple shear flow. Stokes flow, $Ca = 0.6$, $\lambda = 11.7$, $2r_d/L_Y = 0.75$.
(a) Present results (from upper left to lower right: $t = 0$, $t = 15$, $t = 30$, $t = 50$, $t = 57$ and $t = 67$); (b) Experimental results. Reprinted with permission from Vananroye *et al.* (2006). Copyright 2006 American Chemical Society.

4. CONCLUSIONS AND FUTURE WORK

A methodology for simulating multiphase flows was presented in section 2, with an emphasis on simulations of droplet deformation and breakup under simple shear flows. As demonstrated in section 3, this methodology has been validated for a wide range of Capillary numbers, with viscosity ratios ranging from 0.3 to 35. As such, this methodology is capable of dealing with very viscous droplets, as well as droplet breakup phenomena, and displays adequate volume conservation of the dispersed phase, even on coarser meshes.

Future work in this topic will be focused on emulsion rheology and on the study of ferrofluid emulsions. As such, the methodology presented in this work will need to be updated, in order to be capable of accurately simulating magnetic fields, as well as the magnetic effects on ferrofluid droplets.

5. REFERENCES

Albensoeder, S. and Kuhlmann, H., 2005. "Accurate three-dimensional lid-driven cavity flow". *Journal of Computational Physics*, Vol. 206, No. 2, pp. 536 – 558. ISSN 0021-9991. doi:https://doi.org/10.1016/j.jcp.2004.12.024. URL http://www.sciencedirect.com/science/article/pii/S0021999105000033.

Barai, N. and Mandal, N., 2019. "Breakup versus coalescence of closely packed fluid drops in simple shear flows". *International Journal of Multiphase Flow*, Vol. 111, pp. 1–15.

Cox, R., 1969. "The deformation of a drop in a general time-dependent fluid flow". *Journal of fluid mechanics*, Vol. 37, No. 3, pp. 601–623.

Croce, R., Griebel, M. and Schweitzer, M.A., 2010. "Numerical simulation of bubble and droplet deformation by a level set approach with surface tension in three dimensions". *International Journal for numerical methods in fluids*, Vol. 62, No. 9, pp. 963–993.

Cunha, L.H., Siqueira, I.R., Oliveira, T.F. and Ceniceros, H.D., 2018. "Field-induced control of ferrofluid emulsion rheology and droplet break-up in shear flows". *Physics of Fluids*, Vol. 30, No. 12, p. 122110.

Gibou, F., Fedkiw, R. and Osher, S., 2018. "A review of level-set methods and some recent applications". *Journal of Computational Physics*, Vol. 353, pp. 82–109.

Grace, H.P., 1982. "Dispersion phenomena in high viscosity immiscible fluid systems and application of static mixers as dispersion devices in such systems". *Chemical Engineering Communications*, Vol. 14, No. 3-6, pp. 225–277.

Hassan, M.R., Zhang, J. and Wang, C., 2018. "Deformation of a ferrofluid droplet in simple shear flows under uniform magnetic fields". *Physics of Fluids*, Vol. 30, No. 9, p. 092002.

Jiang, G.S. and Shu, C.W., 1996. "Efficient implementation of weighted eno schemes". *Journal of computational physics*, Vol. 126, No. 1, pp. 202–228.

Kennedy, M., Pozrikidis, C. and Skalak, R., 1994. "Motion and deformation of liquid drops, and the rheology of dilute emulsions in simple shear flow". *Computers & fluids*, Vol. 23, No. 2, pp. 251–278.

Kim, J. and Moin, P., 1985. "Application of a fractional-step method to incompressible navier-stokes equations". *Journal of Computational Physics*, Vol. 59, No. 2, pp. 308 – 323. ISSN 0021-9991. doi:https://doi.org/10.1016/0021-9991(85)90148-2. URL http://www.sciencedirect.com/science/article/pii/0021999185901482.

Li, J., Renardy, Y.Y. and Renardy, M., 2000. "Numerical simulation of breakup of a viscous drop in simple shear flow through a volume-of-fluid method". *Physics of Fluids*, Vol. 12, No. 2, pp. 269–282.

Oliveira, T. and Cunha, F., 2015. "Emulsion rheology for steady and oscillatory shear flows at moderate and high viscosity ratio". *Rheologica Acta*, Vol. 54, No. 11-12, pp. 951–971.

Osher, S. and Fedkiw, R., 2006. *Level set methods and dynamic implicit surfaces*, Vol. 153. Springer Science & Business Media.

Osher, S. and Sethian, J.A., 1988. "Fronts propagating with curvature-dependent speed: algorithms based on hamilton-jacobi formulations". *Journal of computational physics*, Vol. 79, No. 1, pp. 12–49.

Peng, D., Merriman, B., Osher, S., Zhao, H. and Kang, M., 1999. "A pde-based fast local level set method". *Journal of computational physics*, Vol. 155, No. 2, pp. 410–438.

Rallison, J., 1981. "A numerical study of the deformation and burst of a viscous drop in general shear flows". *Journal of Fluid Mechanics*, Vol. 109, pp. 465–482.

Shu, C.W. and Osher, S., 1988. "Efficient implementation of essentially non-oscillatory shock-capturing schemes". *Journal of computational physics*, Vol. 77, No. 2, pp. 439–471.

Sussman, M., Fatemi, E., Smereka, P. and Osher, S., 1998. "An improved level set method for incompressible two-phase flows". *Computers and Fluids*, Vol. 27, No. 5, pp. 663 – 680. ISSN 0045-7930. doi:https://doi.org/10.1016/S0045-7930(97)00053-4. URL http://www.sciencedirect.com/science/article/pii/S0045793097000534.

Sussman, M., Smereka, P. and Osher, S., 1994. "A level set approach for computing solutions to incompressible two-phase flow". *Journal of Computational physics*, Vol. 114, No. 1, pp. 146–159.

Taylor, G.I., 1932. "The viscosity of a fluid containing small drops of another fluid". *Proc. R. Soc. Lond. A*, Vol. 138, No. 834, pp. 41–48.

Taylor, G.I., 1934. "The formation of emulsions in definable fields of flow". *Proc. R. Soc. Lond. A*, Vol. 146, No. 858, pp. 501–523.

Vananroye, A., Van Puyvelde, P. and Moldenaers, P., 2006. "Effect of confinement on droplet breakup in sheared emulsions". *Langmuir*, Vol. 22, No. 9, pp. 3972–3974.

Vananroye, A., Van Puyvelde, P. and Moldenaers, P., 2007. "Effect of confinement on the steady-state behavior of single droplets during shear flow". *Journal of rheology*, Vol. 51, No. 1, pp. 139–153.

Vu, T.V., Vu, T.V. and Bui, D.T., 2019. "Numerical study of deformation and breakup of a multi-core compound droplet in simple shear flow". *International Journal of Heat and Mass Transfer*, Vol. 131, pp. 1083–1094.

6. RESPONSIBILITY NOTICE

The authors are the only responsible for the printed material included in this paper.